International Journal of
MATERIALS RESEARCH

Zeitschrift für METALLKUNDE

Original Contributions

Dong He[a], Qiang Li[a], Yu Yan[a], Xiguang Huang[a], Tabassam Yasmeen[b]
[a] School of Mechanical and Materials Engineering, North China University of Technology, Beijing, P.R. China
[b] Department of Mechanical Engineering, Imperial College London, London, UK

Study of plastic deformation mechanisms in TA15 titanium alloy by combination of geometrically necessary and statistically-stored dislocations

This study combines geometrically necessary dislocation analysis and statistically-stored dislocation identification to investigate plastic deformation mechanisms in TA15 titanium alloy. Tensile tests were conducted up to different strains at room temperature. The slip lines were observed and identified using high resolution scanning electron microscopy. Geometrically necessary dislocations were calculated based on strain gradient theories. The statistically-stored dislocations were studied using transmission electron microscopy under two beam conditions. The results indicate that the ratio of <a>-type geometrically necessary dislocation density to <c+a>-type decreases from 5–8 to 1–3 with increasing strain from 0.8 % to 2.0 %. The <a>-type slip is the dominant deformation mechanism at the early stage of plastic deformation, whereas <c+a>-slips become dominant with further increase in deformation strain.

Keywords: Deformation mechanisms; Geometrically necessary dislocation; Slip line; Transmission electron microscopy; Electron backscatter diffraction

1. Introduction

TA15, also known as Ti-6Al-2Zr-1Mo-1V, is a typical near α titanium alloy. The microstructure of TA15 is composed of dominant α lamellae (hexagonal-close-packed, hcp) and a few residual beta phases (body-centered-cubic, bcc) at room temperature [1]. Because of its high specific strength and excellent corrosion resistance at the evaluated temperature, TA15 titanium alloy is preferentially used in aviation and aerospace industries [2–9].

Generally, because of low symmetry of the hcp crystal structure and the special lamella grain morphology, the near α titanium alloy exhibits low tensile ductility, high strength and anisotropic mechanical properties compared to beta and α+β titanium alloy [10]. The deformation mechanisms in hcp metal are complex because of the competition between dislocation slip (including basal, prismatic pyramidal slip model) and twinning under different deformation conditions [11, 12]. Especially, due to a relatively high Al content, twinning in alloyed TA15 tends to be suppressed and dislocation slip is the dominant plastic deformation mechanism. According to von-Mises criterion, at least five independent slip systems are required for homogeneous plastic deformation. Therefore, in addition to basal $<11\bar{2}0>\{0002\}$, prismatic $<11\bar{2}0>\{10\bar{1}0\}$ and pyramidal $<11\bar{2}0>\{10\bar{1}1\}$ slip modes, the non-basal <c+a> $<11\bar{2}3>\{10\bar{1}1\}$ and/or $\{11\bar{2}2\}<11\bar{2}3>$ slips are invoked [13]. However, the effect of addition slip modes on full plastic deformation of titanium and titanium alloys is still debatable [14]. Therefore, it is very important to study deformation mecha-

nisms of TA15 titanium alloy by combination of geometrically necessary dislocations (GNDs) and statistically-stored dislocations (SSDs).

Stored dislocations in metallic materials can be separated into two categories: SSDs and GNDs. SSDs are generated by trapping each other in a random way and are dependent on effective plastic strain. GNDs are the stored dislocations that relieve plastic deformation incompatibilities within the material caused by non-uniform dislocation slip. The density of GNDs is directly proportional to the strain gradients [15].

The SSD configurations and types can be studied using transmission electron microscopy (TEM) under two beam conditions [16, 17]. The GND contents also can be resolved through the detected lattice rotations based on strain gradient theories and Nye [18], Ashby [15] and Kroner's work [19], which can be used to understand the local deformation mechanism [20–23]. Very recently, Wilkinson et al. [24–30] have developed a cross-correlation-based analysis of electron backscatter diffraction (EBSD) patterns, which can improve the sensitivity by approximately two orders of magnitude.

In the present work, ex-situ uniaxial tensile deformation is performed on TA15 titanium alloy at room temperature. Scanning electron microscopy (SEM) measurements are conducted to reveal slip trace natures at different strains. EBSD measurements with patterns recorded simultaneously at every scanning point are carried out. GND contents are calculated by using cross-correlation-based analysis (self-developed routines within MatLab). The SSD types (Burgers vector) are identified by TEM under two beam conditions. Finally, the micro-mechanism of plastic deformation in TA15 titanium alloy is analyzed by combination of GNDs and SSDs.

2. Experimental procedure and calculation method

2.1. Materials and sample preparation

TA15 titanium bar stock with a chemical composition of 6.47 wt.% Al, 1.59 wt.% Zr, 1.45 wt.% Mo, 1.91 wt.% V, 0.038 wt.% Fe and balance titanium was used in the present study. The as-received material was subjected to β forging at 1050 °C and was subsequently annealed at 600 °C for 4 h. The microstructure of the used alloy consisted of lamellar primary α phase and residual β phase (less than 10 vol.%), as seen in Fig. 1.

Flat tensile samples of 65 mm in length and 1 mm in thickness were machined from the TA15 alloy wrought bars. The gauge length of the tensile sample was 50 mm.

The flat surfaces of the tensile samples were prepared for SEM/EBSD measurements through standard grinding and polishing routines. The final polishing was performed with a polishing solution consisting of colloidal silica (PO-S, 90 vol.%) and H_2O_2 (10 vol.%).

2.2. Tensile tests and SEM/EBSD measurements

Two tensile tests, labeled as "sample A" and "sample B", were performed at the same strain rate (1.0×10^{-4} s^{-1}). Tensile tests of samples A and B were conducted up to macroscopic strains of 0.8 % and 2.0 %, respectively. The polished surfaces of the tensile samples were carefully protected during the tensile test for subsequent slip traces observation and EBSD measurement.

The SEM/EBSD measurements were carried out on a JEOL-6500F SEM equipped with an EBSD system developed by EDAX/TSL® at 20 kV and using a probe current

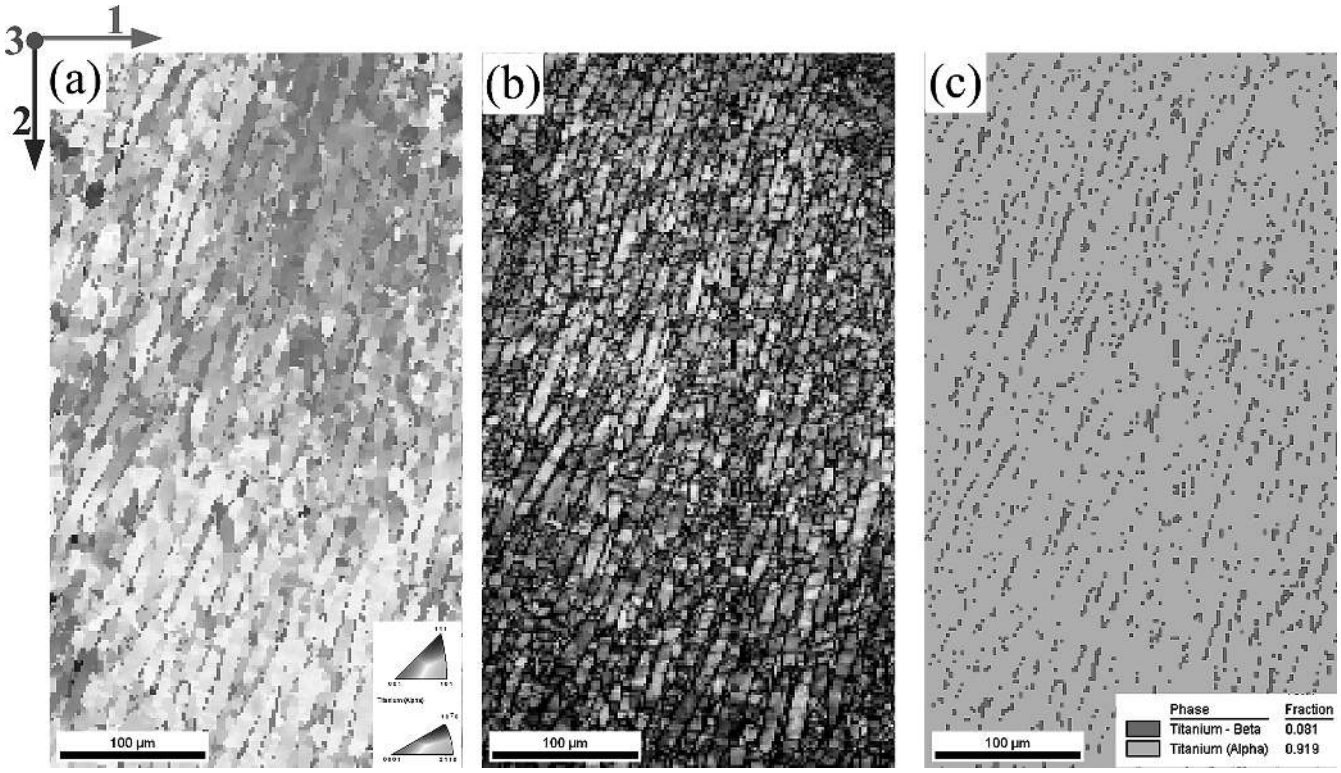

Fig. 1. EBSD maps of the initial microstructure of TA15 titanium alloy: (a) Inverse pole figure (IPF) map, scanning step size: 0.5 µm; (b) Corresponding image quality map; (c) Corresponding phase map.

of approximately 1 nA. EBSD scanning was conducted in the selected interesting zones using a square grid with a step size of 0.2 μm. The Kikuchi diffraction patterns were simultaneously captured at 1×1 binning and recorded to disk for subsequent GND calculation.

2.3. Cross-correlation-based method and GND density calculation

In the current study, the cross-correlation-based method [30] was applied to get the displacement gradient tensor. Here, the displacement gradient tensor was conducted on CrossCourt V3 (BLG productions Ltd., Bristol UK, www.blgprodctions.co.uk) commercial software.

GND density and content were calculated based on the displacement gradient tensor using self-developed routines within MatLab (The MathworksInc., www.mathworks.-com). In α titanium alloys, there are 24 groups of known possible independent slip systems [31], as follows: 3 groups of <a>-basal, 3 groups of <a>-prismatic, 6 groups of <a>-pyramidal and 12 groups of <c+a> pyramidal slip systems. Then, 33 types of potential dislocations were taken into account for the calculation of GND density (see references [31, 32]). L1-norm [27, 33], defined as Eq. (1), was used in the calculations and a lower bound estimate of the GND content was determined by self-developed routines.

$$L^1 = \sum_{k=1}^{m} \left| \rho_{\text{gnd}}^k w^k \right| \tag{1}$$

where ρ_{gnd}^k is the individual GND density in the k-th slip system; w^k is the weight factor for ρ_{gnd}^k, and m is the total number of slip systems.

Weight factor of w is defined by Eq. (2) [21]:

$$w^k = c\mu (b^k)^2 \tag{2}$$

Where μ is 1 for screw dislocations and $1/(1-v)$ for edge dislocations (where v is Poisson's ratio); c is a constant.

For α titanium, the Burgers vector magnitude was $b = 2.95 \times 10^{-10}$ m for <a> type slip and 5.53×10^{-10} m for <c+a> type slip [34]. The different weight factors for different dislocation types used in the current study are calculated and listed in Table 1.

2.4. TEM measurement and dislocation type identification

TEM measurements under two beam conditions were carried out on a Tecnai G2-F30 operating at 200 kV using a standard double-tilt holder. The TEM images were obtained in bright field mode under two beam condition tilted off the same zone axis but with different diffraction vectors ($\vec{g}$) to identify the dislocation type. The dislocation type was identified using the $\vec{g} \cdot \vec{b}$ criterion: if $\vec{g} \cdot \vec{b} = 0$, the dislocation line is not visible; otherwise, the dislocation is visible. This enables the Burgers vector determination and identification of the dislocation type by taking images of the same sample area by exploiting different $\vec{g}$. As mentioned above, there are three types of full dislocations in α titanium, as follows: <a>, <c> and <c+a>-type [35]. The $\vec{g} \cdot \vec{b}$ criterion under [01$\bar{1}$0] zone axes in α titanium is presented in Table 2.

3. Results and discussion

3.1. Slip line morphology and distribution

For sample A with 0.8 % tensile strain, basal and prismatic slip system activations were detected in the selected α grains, which possess relatively high basal or prismatic slip Schmid factors (SFs), as shown in Fig. 2 and Table 3. At this deformation stage, the slip lines are straight and relatively fine (see the grains labeled 1, 2, and 8 in Fig. 2a). The slip lines show an almost equidistant distribution in the α grains. The slip lines originate from grain/phase boundaries and gradually extend into the grain interior. Two equivalent {10$\bar{1}$0}<11$\bar{2}$0> slip system traces are additionally presented in some α grains (see grains 3 and 4 in Fig. 2a).

However, the distributions of slip lines in the observed zone are heterogeneous. No obvious slip traces were detected in some α grains, such as grains 5 and 6 in Fig. 2a, which also possess relative high SFs for basal or prismatic slip. These results indicate that, for polycrystals/multiphase materials, the slip system activations are not only determined by the relationships between crystallographic orientation and load axis, but other factors, such as grain morphology, neighbor phase and grains distribution, also play an important role.

Although the deformation strain is very small (Sample A, 0.8 % tensile strain), the slip is not constrained to one grain.

Table 2. $\vec{g} \cdot \vec{b}$ criterion under [<01$\bar{1}$0>] zone axes in α titanium.

$\vec{g}$	<a>	<c>	<c+a>
	1/3<11$\bar{2}$0>	<0001>	1/3<11$\bar{2}$3>
<0002>	invisible	visible	visible
<$\bar{2}$112>	visible	visible	Partial visible
<$\bar{2}$110>	visible	invisible	visible

Table 1. Potential dislocation types and weight factors in α titanium.

Slip system	Burgers vector	Edge		Screw	
		Number	Weight	Number	Weight
<a>-basal	<11$\bar{2}$0>	3	0.124	3	0.087
<a>-prismatic	<11$\bar{2}$0>	3	0.124	0	–
<a>-pyramidal	<11$\bar{2}$0>	6	0.124	0	–
<c+a>-pyramidal	<11$\bar{2}$3>	12	0.437	6	0.306

Slip transmission phenomenon is observed in some regions, as shown in Fig. 2c. It shows clearly that slip transfers from one α lamella (labeled a) into another neighboring α grain (labeled b) by activating the related slip system of the β layer (labeled o) between them. This result is different from Bridier group's work on slip line morphology observation during Ti-6Al-4V in situ tensile deformation, which indicates that the slip line is limited to one grain at small deformation stage [36]. There are two possible reasons for the difference. First, the studied TA15 titanium alloy is a near α titanium alloy, which contains only 8.1 % β phase (volume fraction). Thus, the β layer is relatively thin and the slip is easy to transfer in comparison with α/β Ti-6Al-4V. Second, the Burgers orientation relationship (OR) ($\{0001\}_\alpha \| \{110\}_\beta$, $\langle 11\bar{2}0\rangle_\alpha \| \langle 111\rangle_\beta$) is fully maintained between α lamellae (labeled a and b) and β layer (labeled o) (see Fig. 2d). This special OR may facilitate the slip transmission [37, 38].

The nature and distribution of gliding of sample B evolves significantly with increasing tensile strain. More α grains have been activated compared with sample A, as shown in Fig. 3a. Basal and prismatic slip systems are still the dominant deformation modes for α grains in the observed region. A few first-order pyramidal glides are also detected in some α grains, whose SFs for basal and prismatic slip systems are relatively low.

The slip lines are still generally straight, but their distributions are much more intensive compared with sample A.

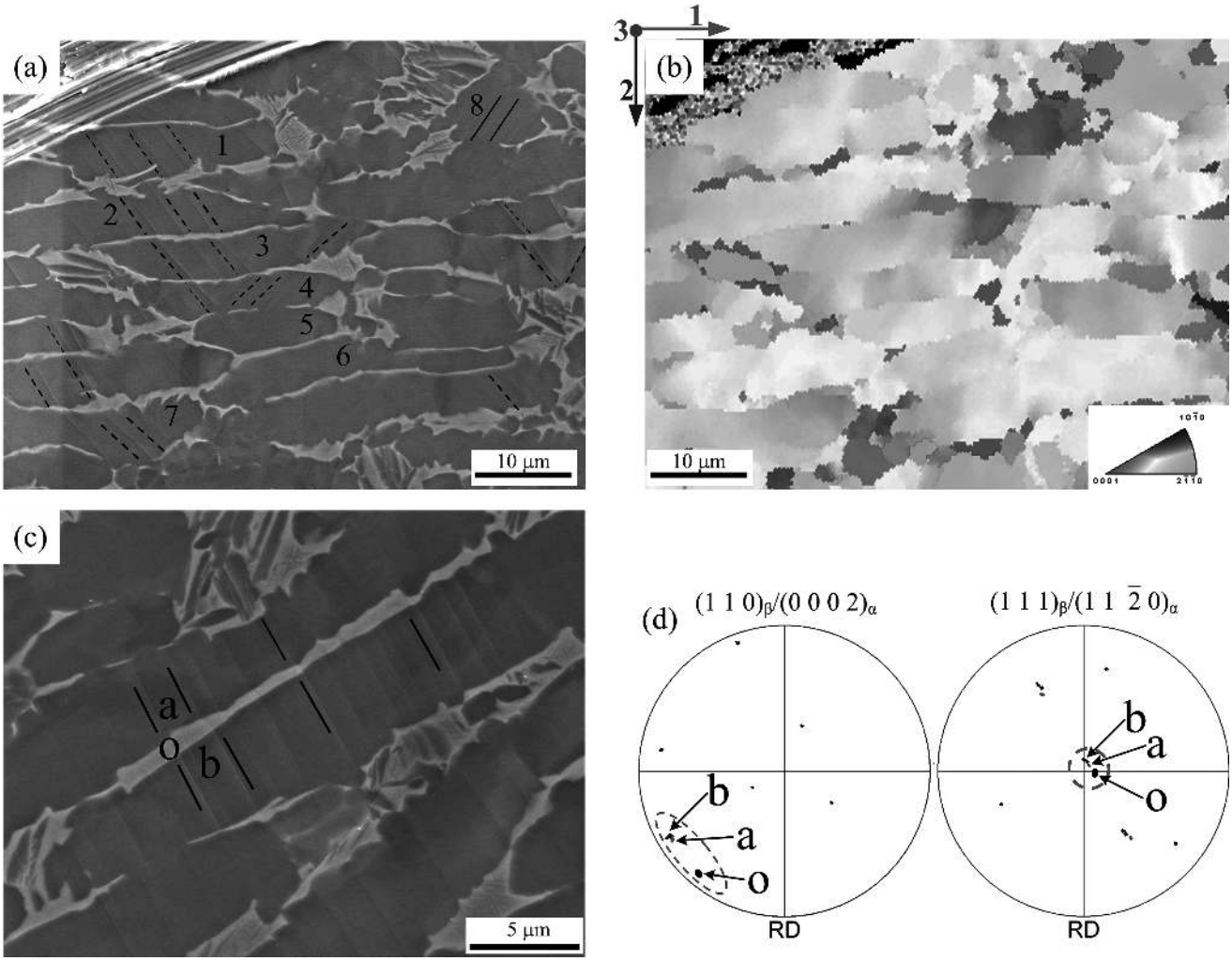

Fig. 2. Slip line morphology, distribution and identification of sample A with 0.8 % tensile strain. Continuous and dotted black lines represent the calculated traces of basal and prismatic slip systems, respectively. (a) SEM image and slip line identification; (b) IPF map corresponding to Fig. 2a, step size 0.4 μm; (c) SEM image with higher magnification and slip line identification; (d) $\{110\}_\beta/\{0002\}_\alpha$ and $\{111\}_\beta/\{11\bar{2}0\}_\alpha$ pole figures of α lamellae (labeled a, b) and thin β layers (labeled o) in Fig. 2c.

Table 3. The Schmid factors of the labelled grains presented in Fig. 2a.

Grain No.	1	2	3	4	5	6	7	8
SF for basal	0.1 ~ 0.3	0.2 ~ 0.3	0.05 ~ 0.15	0.05 ~ 0.15	0.05 ~ 0.18	0.15 ~ 0.2	0.1 ~ 0.2	0.47 ~ 0.5
SF for prismatic	0.42 ~ 0.46	0.45 ~ 0.475	0.45 ~ 0.5	0.40 ~ 0.47	0.43 ~ 0.47	0.42 ~ 0.45	0.43 ~ 0.47	0.15 ~ 0.2

However, there are still several α grains in which no obvious slip system activation has been detected.

In some α grains, which possess relative high SFs for both basal and prismatic slip systems, "pencil" slip line morphology appeared (see Fig. 3b), and this phenomenon is usually observed in bcc materials upon tensile deformation. This morphology results from the coexistence of basal and prismatic slip systems in one grain. These results indicate that the slip model gradually transforms from uniserial to multi serial slip, as deformation strain increases.

3.2. GND content and density

The GND content and density maps within selected regions on sample A and B are presented in Fig. 4. The microstructures within the investigated region are composed of lamellar and equiaxed α grains, as seen in Fig. 4a and d.

For sample A, which was subjected to 0.8 % tensile strain, the mean value of total GND density for the solved pixels reaches 9.70×10^{14} m^{-2}. The total GND density distribution shows obvious heterogeneity. The GND density

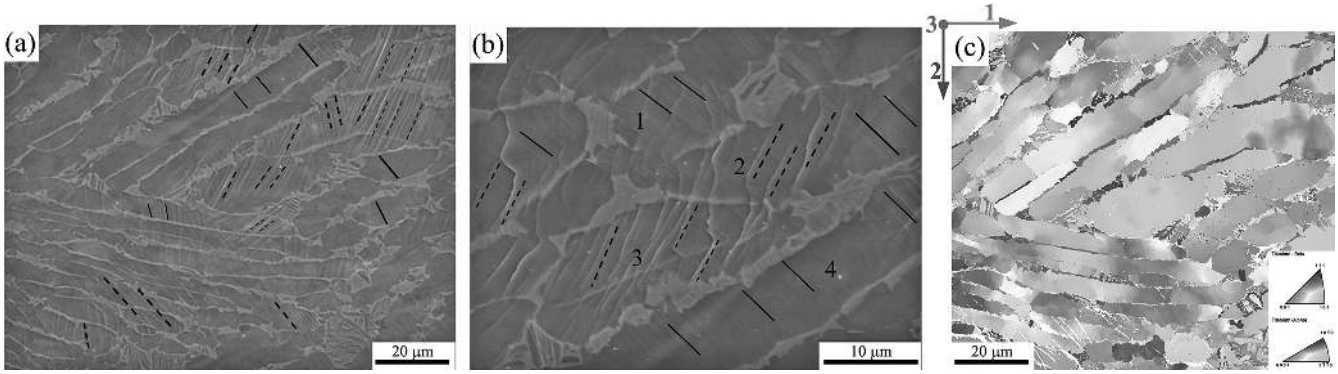

Fig. 3. Slip line morphology, distribution and identification of sample B with 2.0 % tensile strain. Continuous and dotted black lines represent the calculated traces of basal and prismatic slip systems, respectively. (a) SEM image and slip line identification; (b) SEM image with higher magnification and slip line identification; (c) IPF map corresponding to Fig. 3a, step size 0.2 μm.

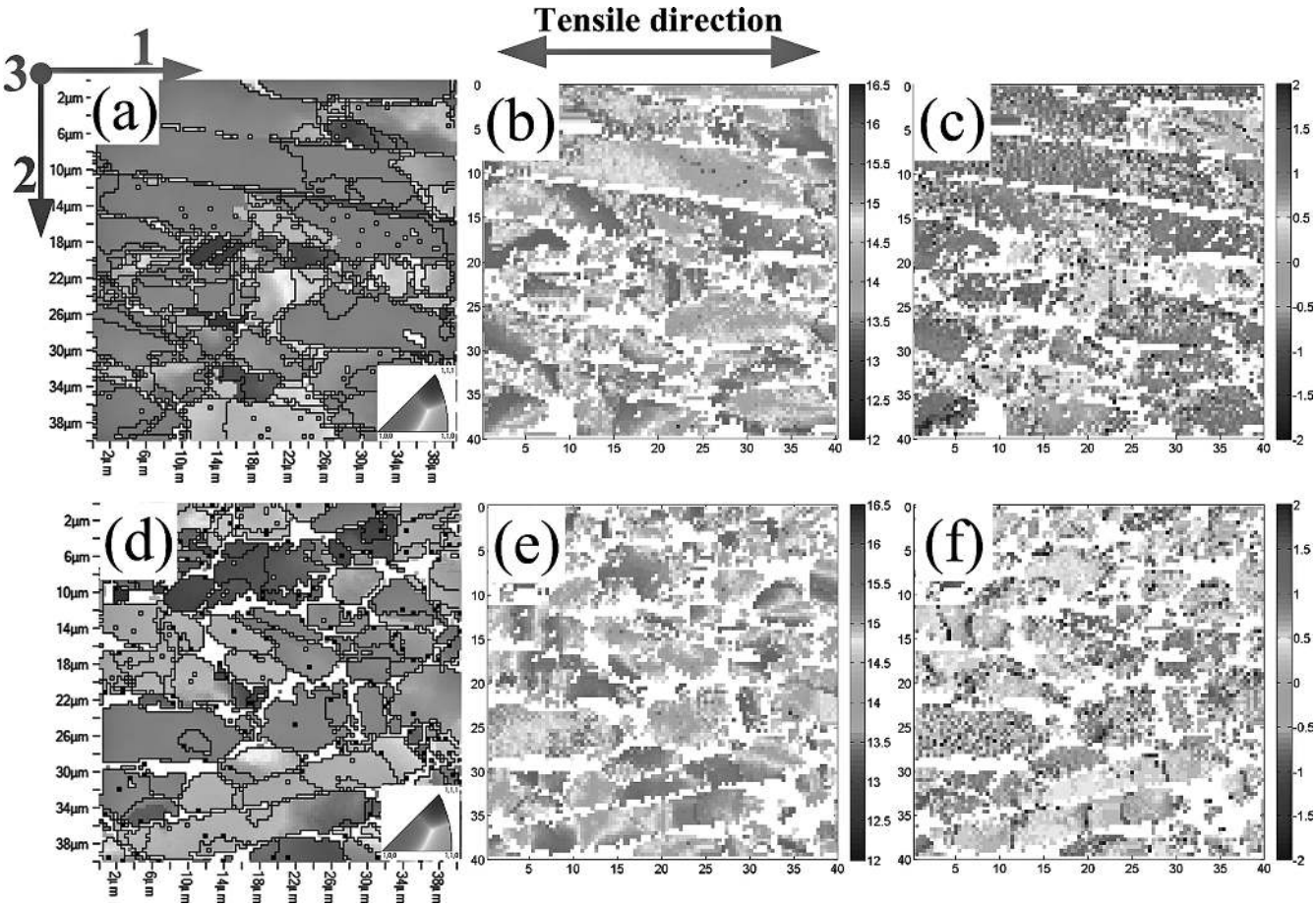

Fig. 4. hcp deconstructions of the GND density distribution of TA15 titanium with different tensile strains: (a), (d) Orientation microscopy map of TA15 titanium alloy, scanning step size: 0.2 μm; (b), (e) Total GND density, the gray-scale is log10(ρ), with ρ in m^{-2} ; (c), (f) Ratio of <a>-type GND density to <c+a>-type (Log gray-scale).

around (sub)grain or phase boundary is much higher compared with grain interior, as seen in Fig. 4b. The plastic deformation strain is mainly concentrated around the grain/phase boundary at the early stage of plastic deformation. This finding is consistent with the results mentioned in the last section that the slip lines originate from grain/phase boundaries.

To facilitate the analysis of contributions from different types of GNDs, the total density is separated into <a>- and <c+a>-type GNDs. The ratio of <a>-type to <c+a>-type GND density (Log grey-scale) is displayed in Fig. 4c. The <a>-type GNDs have obvious superiority to <c+a>-type GNDs in terms of density. The <a>-type GND has about 5 – 8 times higher density than <c+a>-type in most observed regions. These results demonstrate that the <a>-type slip is the dominant mechanism during the TA15 plastic deformation process. There are two possible reasons accounting for it. First, the line energy for <c+a>-type GNDs is about 3.5 times greater than for the <a>-type because of the different magnitudes of Burgers vectors [34]. Second, critical resolved shear stresses for <c+a>-type slips are much higher than <a>-type slips [30].

At higher deformation strain the quality and identification ratio of EBSD patterns are gradually decreased in the thin or small size grain/phase zones, as shown in Fig. 4d. When the tensile strain reaches 2.0 %, the mean value of total GND density is 9.82×10^{14} m^{-2} in the scanned zone of sample B. This means that the total GNDs of sample B is not significantly higher than for sample A. This is because GNDs are related to the local strain gradient field and appear due to geometrical constraints of the crystal lattice [33].

However, for sample B with a larger plastic strain (2.0 %), the ratio of <a>-type GND density to <c+a> is obviously lower than sample A. That of the <a>-type GND is only 1 – 3 times higher than that of <c+a>-type in most regions. The GND distribution in sample B is also more homogeneous than that in sample A. These results demonstrate that with increasing plastic deformation strain, an increasing number of <c+a>-type slips is activated to associate the plastic deformation, although the <a>-type slip is still the dominant activation slip system.

3.3. SSD configuration and identification

The SSD evolutions of TA15 titanium with different tensile strains are presented in Fig. 5. The SSDs are rectilinear and parallel before deformation, as seen in Fig. 5a. With increasing plastic deformation and because of dislocation moving, interaction and multiplication, the configurations of SSDs gradually evolved to dislocation walls or cell substructures (see Fig. 5b and c). The dislocation density increases significantly (Fig. 5b) and its distribution is relatively heterogeneous (Fig. 5c). These results agree well with the experimental study of Ti-6Al-4V [39] and show a similar trend to the GND distributions mentioned above.

The TEM images taken under two beam conditions are presented in Figs. 6 and 7. The dislocation types are identified using the $\vec{g} \cdot \vec{b}$ criterion. For sample A with 0.8 % tensile strain, many <a>-type SSDs were detected and cell substructures are presented under $\vec{g} = [\bar{2}110]$ (see the black arrows indicated in Fig. 6c). The <a>-type SSD density is relatively high and its arrangement is presented as a cell substructure. These results indicate that the <a>-type SSDs are heavily propagated during plastic deformation. However, although few <c>-type SSD lines have been detected (see the white arrows indicated in Fig. 6a), they are almost rectilinear and with no obvious propagation. These results validate the GND analysis and confirm that, for TA15 titanium at room temperature, the <a>-type glide is the dominant mechanism at the early stages of plastic deformation.

For sample B subjected to 2.0 % tensile strain, <c+a>-type SSD density increases significantly (see the long white arrows indicated in Fig. 7a). Furthermore, most of the <c+a>-type dislocation lines are curved and some of them are even tangled together. This demonstrates that many <c+a>-type slips have been activated as deformation strain increases.

Obviously, these results of SSD evolution revealed by TEM using a two beam technique and invisibility criterion agree well with the previous GND calculation results.

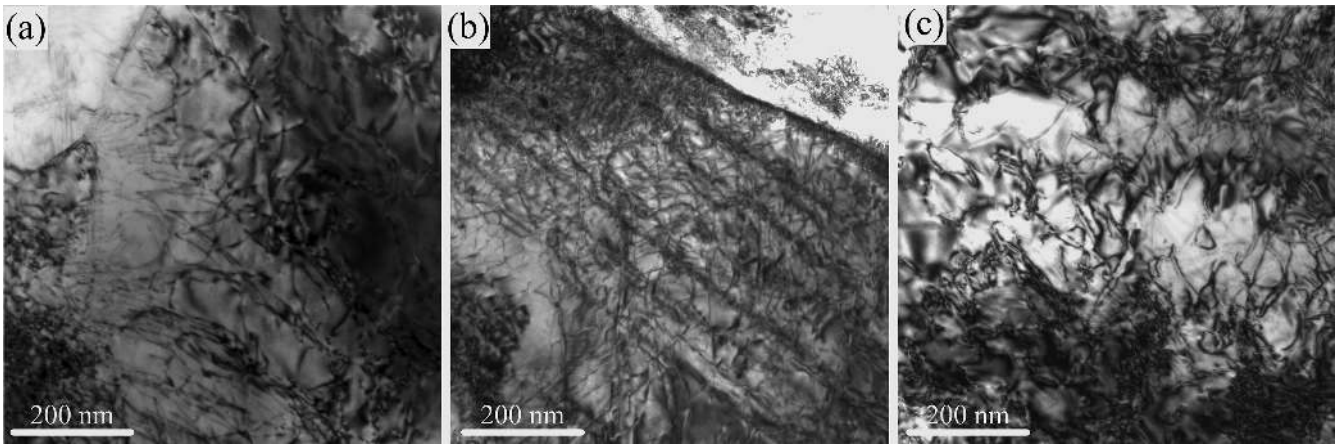

Fig. 5. Dislocation configurations of TA15 titanium with different plastic strain: (a) without deformation; (b) with 0.8 % tensile strain; (c) with 2.0 % tensile strain.

4. Conclusions

By combination of high resolution SEM/EBSD measurements and two beam TEM techniques the activation of slip systems, GND density distribution and SSD identification are investigated on TA15 titanium subjected to different tensile strains. Based on the experimental results and analysis, the following conclusions can be drawn:

1. Slip lines mainly originate from grain/phase boundaries and gradually extend into the grain interior during plastic deformation. The slip type gradually changes from uniserial (basal or prismatic slipping) to multi-serial slipping.
2. The slip lines are not constrained to one grain but transfer from one α lamella to another neighboring α grain by activating the related slip system of β layer even at small deformation stage.
3. Total GND densities are not notably increased as tensile deformation increased from 0.8 % to 2.0 %. However, the GND contents are significantly changed, i. e., <a>-type GNDs have about 5 – 8 times higher content than <c+a>-type at 0.8 % strain but have only 1 – 3 times higher content at 2.0 % strain..
4. Cell-like <a>-type SSDs were detected by TEM under two beam conditions and a few rectilinear <c+a>-type SSDs lines are presented in sample A with 0.8 % deformation strain. The <c+a>-type dislocation lines are curved or even tangled together as the deformation strain increases to 2.0 %.
5. For TA15 titanium at room temperature, the <a>-type glide is the dominant deformation mechanism at the early stage of plastic deformation but many <c+a>-type slips are activated to associate the plastic deformation as deformation strain increases.

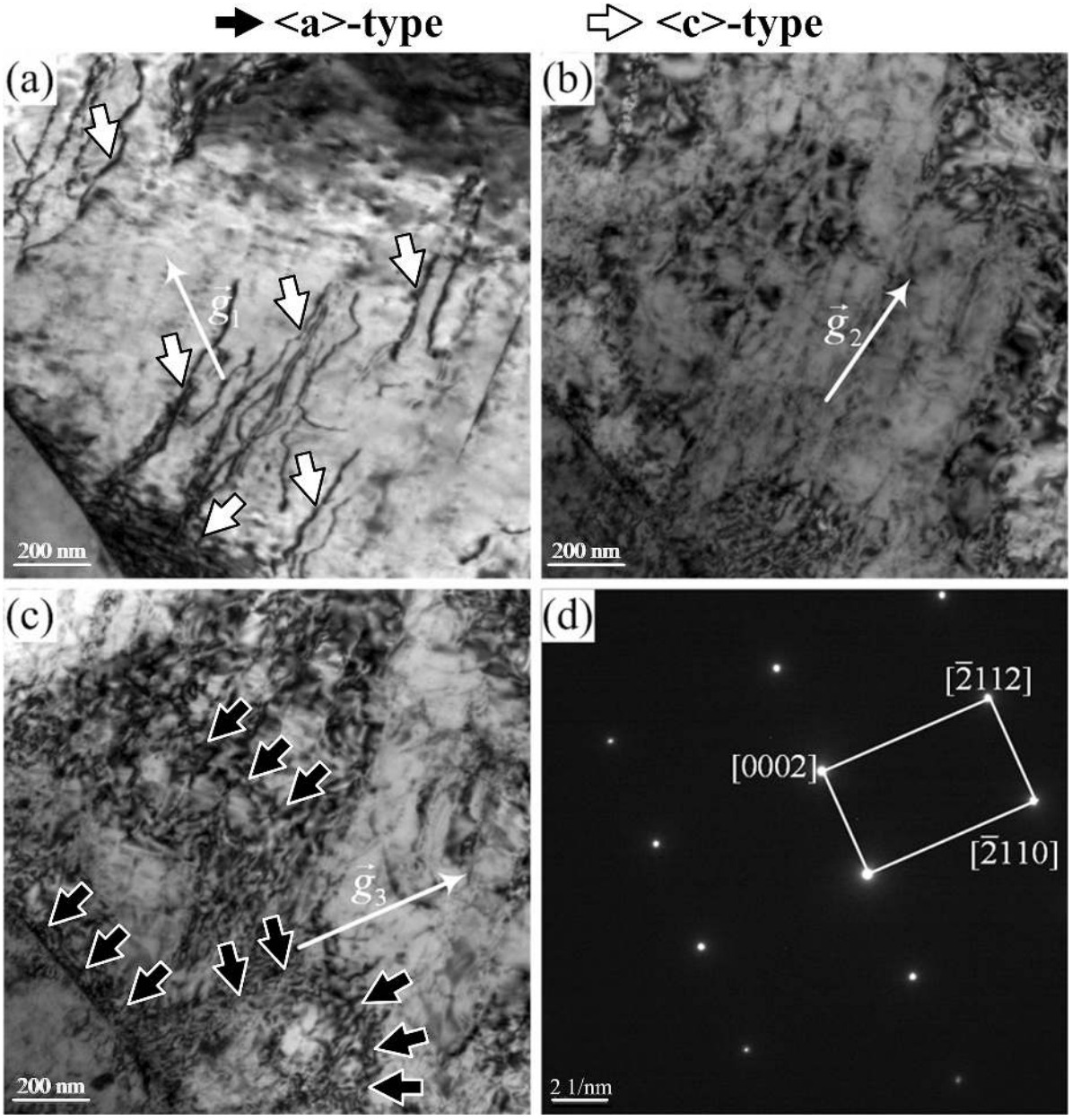

Fig. 6. TEM images of the same region on sample A (with 0.8 % tensile strain) under two beam conditions: (a) $\vec{g}$ = [0002]; (b) $\vec{g}$ = [$\bar{2}$112]; (c) $\vec{g}$ = [$\bar{2}$110]; (d) corresponding diffraction pattern.

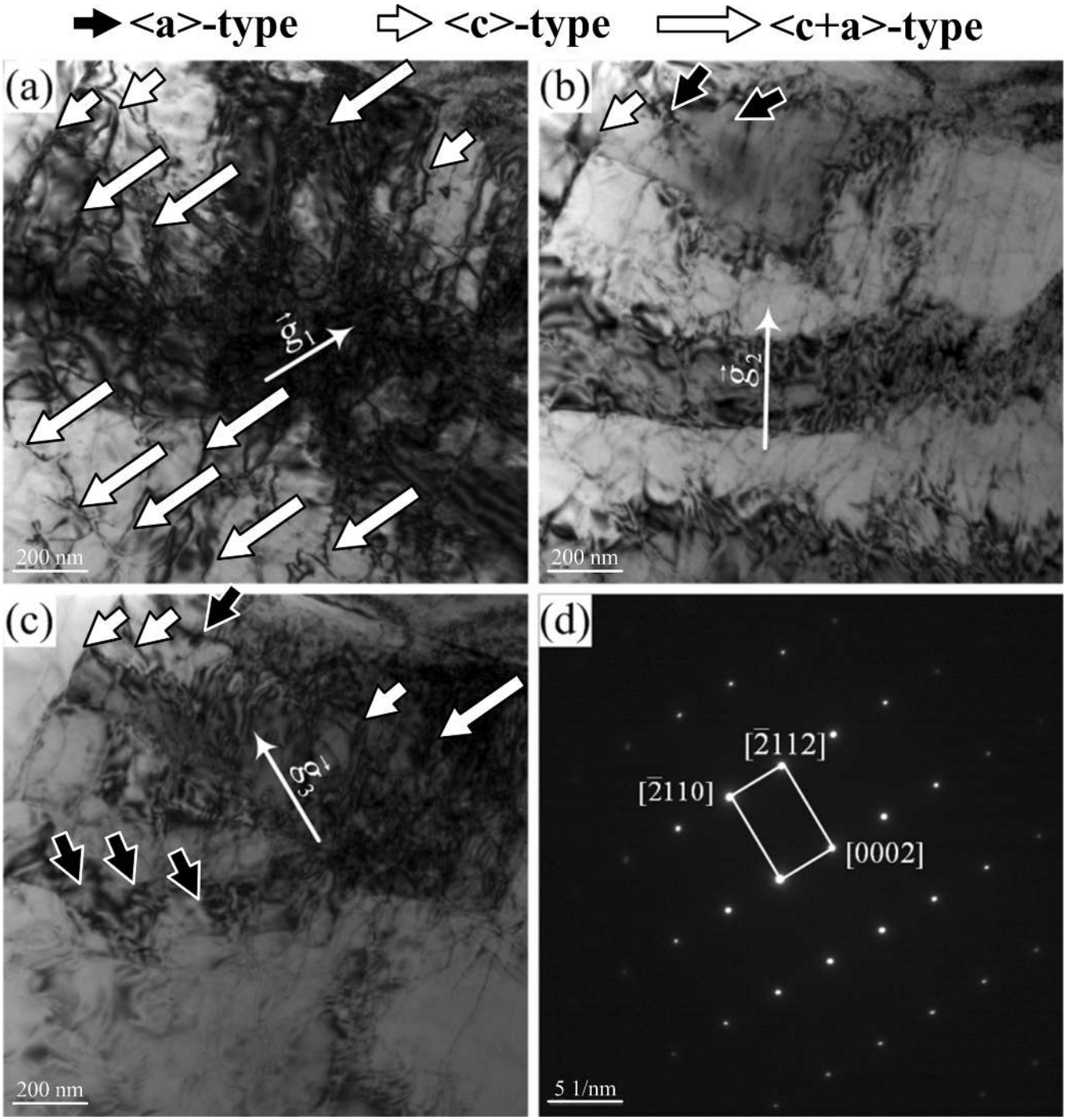

Fig. 7. TEM images of the same region on sample B (with 2.0% tensile strain) under two beam conditions: (a) $\vec{g}$ = [0002]; (b) $\vec{g}$ = [$\bar{2}$112]; (c) $\vec{g}$ = [$\bar{2}$110]; (d) corresponding diffraction pattern.

The author (He Dong) gratefully acknowledges the financial support by National Natural Science Foundation of China under contract (No. 51401226), Outstanding Young Scholars Foundation (XN071010) and Startup Fund Program of North China University of Technology.

References

[1] D. He, J.C. Zhu, S. Zaefferer, D. Raabe, Y. Liu, Z.H. Lai, X.W. Yang: Mater. Sci. Eng. A 549 (2012) 20. DOI:10.1016/j.msea.2012.03.110
[2] M.J. Donachie: Titanium – A technical guide, ASM International, Ohio, USA (1988).
[3] P.F. Gao, H. Yang, X.G. Fan, S.L. Yan: Mater. Sci. Eng. A 540 (2012) 245. DOI:10.1016/j.msea.2012.02.006
[4] Z.C. Sun, H. Yang, G.J. Han, X.G. Fan: Mater. Sci. Eng. A 527 (2010) 3464. DOI:10.1016/j.msea.2010.02.009
[5] Z.L. Zhao, H.Z. Guo, L. Chen, Z.K. Yao: Rare Metals 28 (2009) 523. DOI:10.1007/s12598-009-0101-8
[6] Z.J. Wang, H. Song: J. Alloys Compd. 470 (2009) 522. DOI:10.1016/j.jallcom.2008.03.027
[7] Z.C. Sun, H. Yang: Mater. Sci. Eng. A 523 (2009) 184. DOI:10.1016/j.msea.2009.05.058
[8] Y. Liu, J.C. Zhu, Y. Wang: Rare Metal Mat. Eng. 38 (2009) 1390. DOI:10.3321/j.issn:1002-185X
[9] Y. Wang, J.C. Zhu, Y. Liu, Z.H. Lai: J. Cent. South Univ. Technol. 14 (2007) 90. DOI:10.1007/s11771-007-0339-y

[10] S. Nemat-Nasser, W.G. Guo, J.Y. Cheng: Acta Mater. 47 (1999) 3705. DOI:10.1016/S1359-6454(99)00203-7
[11] N.P. Gurao, R. Kapoor, S. Suwas: Acta Mater. 59 (2011) 3431. DOI:10.1016/j.actamat.2011.02.018
[12] G. Chin, W. Mammel: Metall. Mater. Trans. B 1 (1970) 357. DOI:10.1007/BF02811542
[13] J.R. Cho, D. Dye, K.T. Conlon, M.R. Daymond, R.C. Reed: Acta Mater. 50 (2002) 4847. DOI:10.1016/S1359-6454(02)00354-3
[14] M. Yoo, J. Morris, K. Ho, S. Agnew: Metall. Mater. Trans. A 33 (2002) 813. DOI:10.1007/s11661-002-0150-1
[15] M.F. Ashby: Philos. Mag. 21 (1970) 399. DOI:10.1080/14786437008238426
[16] Y. Ishida, H. Ishida, K. Kohra, H. Ichinose: Philos. Mag. A 42 (1980) 453. DOI:10.1080/01418618008239369
[17] G.S. Liu, I.M. Robertson: J. Mater. Res. 26 (2011) 514. DOI:10.1557/jmr.2010.83
[18] J.F. Nye: Acta Metall. 1 (1953) 153. DOI:10.1016/0001-6160(53)90054-6
[19] E. Kroner: Statistical continuum mechanics, Springer Verlag, New York (1971). DOI:10.1007/978-3-7091-2862-6
[20] J.W. Kysar, Y.X. Gan, T.L. Morse, X. Chen, M.E. Jones: J. Mech. Phys. Solids 55 (2007) 1554. DOI:10.1016/j.jmps.2006.09.009
[21] J.W. Kysar, Y. Saito, M.S. Oztop, D. Lee, W.T. Huh: Int. J. Plast. 26 (2010) 1097. DOI:10.1016/j.ijplas.2010.03.009
[22] H. Liang, F.P.E. Dunne: Int. J. Mech. Sci. 51 (2009) 326. DOI:10.1016/j.ijmecsci.2009.03.005
[23] E. Demir, D. Raabe, N. Zaafarani, S. Zaefferer: Acta Mater. 57 (2009) 559. DOI:10.1016/j.actamat.2008.09.039
[24] A.J. Wilkinson, G. Meaden, D.J. Dingley: Mater. Sci. Technol. 22 (2006) 1271. DOI:10.1179/174328406X130966
[25] A.J. Wilkinson, G. Meaden, D.J. Dingley: Ultramicroscopy 106 (2006) 307. DOI:10.1016/j.ultramic.2005.10.001
[26] D.J. Dingley: J. Microsc. 213 (2004) 214. DOI:10.1111/j.0022-2720.2004.01321.x
[27] S. Sun, B.L. Adams, W.E. King: Philos. Mag. A 80 (2000) 9. DOI:10.1080/01418610008212038
[28] B.S. El-Dasher, B.L. Adams, A.D. Rollett: Scr. Mater. 48 (2003) 141. DOI:10.1016/S1359-6462(02)00340-8
[29] M. Kamaya, A.J. Wilkinson, J.M. Titchmarsh: Nucl. Eng. Des. 235 (2005) 713. DOI:10.1016/j.nucengdes.2004.11.006
[30] T.B. Britton, S. Birosca, M. Preuss, A.J. Wilkinson: Scr. Mater. 62 (2010) 639. DOI:10.1016/j.scriptamat.2010.01.010
[31] I.P. Jones, W.B. Hutchinson: Acta Metall. 29 (1981) 951. DOI:10.1016/0001-6160(81)90049-3
[32] S. Zaefferer: Mater. Sci. Eng. A 344 (2003) 20. DOI:10.1016/S0921-5093(02)00421-5
[33] A. Arsenlis, D.M. Parks: Acta Mater. 47 (1999) 1597. DOI:10.1016/S1359-6454(99)00020-8
[34] T.B. Britton, H. Liang, F.P.E. Dunne, A.J. Wilkinson: Proc. R. Soc. London, Ser. A 466 (2010) 695. DOI:10.1098/rspa.2009.0455
[35] C. Leyens, M. Peters: Titanium and Titanium Alloys, Wiley-VCH Verlag GmbH & Co., Weinheim, Germany (2003). DOI:10.1002/3527602119
[36] F. Bridier, P. Villechaise, J. Mendez: Acta Mater. 53 (2005) 555. DOI:10.1016/j.actamat.2004.09.040
[37] S. Suri, G.B. Viswanathan, T. Neeraj, D.H. Hou, M.J. Mills: Acta Mater. 47 (1999) 1019. DOI:10.1016/S1359-6454(98)00364-4
[38] D. He, J. Zhu, S. Zaefferer, D. Raabe: Mater. Des. 56 (2014) 937. DOI:10.1016/j.matdes.2013.12.018
[39] P. Castany, F. Pettinari-Sturmel, J. Crestou, J. Douin, A. Coujou: Acta Mater. 55 (2007) 6284. DOI:10.1016/j.actamat.2007.07.032

(Received April 17, 2016; accepted August 12, 2016; online since October 24, 2016)

Correspondence address

Dr. Dong He
School of Mechanical and Materials Engineering
North China University of Technology
No. 5, Jingyuanzhuang Road
Beijing 100144
P. R. China
Tel.: +86-10-88801821
Fax: +86-10-88801821
E-mail: hedong@ncut.edu.cn

Bibliography
DOI 10.3139/146.111438
Int. J. Mater. Res. (formerly Z. Metallkd.)
107 (2016) 12; page 1073 – 1081

ISSN 1862-5282